Second-harmonic scattering in aqueous urea solutions: Evidence for solute clusters?

Second-harmonic scattering in aqueous urea solutions: evidence for solute clusters?†

Martin R. Ward,[1] Stanley W. Botchway,[2] Andrew D. Ward[2] and Andrew J. Alexander[1]*

[1]*School of Chemistry, University of Edinburgh, Edinburgh, Scotland, EH9 3JJ*

[2]*STFC, Rutherford Appleton Laboratory, R92, Harwell-Oxford, Oxfordshire, OX11 OQX*

**e-mail: andrew.alexander@ed.ac.uk*

†Celebrating 300 years of Chemistry at Edinburgh

Abstract

Measurements of second-harmonic scattering (SHS) from concentrated aqueous solutions of urea are reported for the first time using scanning microscopy. SHS signal was measured as a function of solution concentration (C) over a range of saturation conditions from undersaturated (S = 0.15) to supersaturated (S = 1.86), where $S = C/C_{sat}$ and C_{sat} is the saturation concentration. The results show a non-linear increase in SHS signal against concentration, with local maxima near S = 0.95 and 1.75 suggesting a change in solution structure near these points. Rayleigh scattering images indicate the presence of particles in nearly saturated (S = 0.95) urea solutions. Time-dependent SHS measurements indicate that signals originate from individual events encountered during scanning of the focal volume through the solution, consistent with second harmonic generation (SHG) from particles. SHG from aqueous dispersions of barium titanate ($BaTiO_3$) nanoparticles with diameters < 200 nm, showed signals ~20 times larger than urea solutions. The results suggest the existence of a population of semi-ordered clusters of urea that changes with solution concentration.

1. Introduction

Nucleation, the process of formation of a new phase from an existing phase, is of fundamental scientific interest. It is also tremendously important economically because it is used, for example, in the production of agrochemicals, cosmetics, foods, and pharmaceuticals. Spontaneous nucleation is often referred to as primary nucleation, in contrast to secondary nucleation which requires a seed of the new phase.[1] Nucleation can also be classed as homogeneous or heterogeneous depending on whether the new phase nucleates alone or on the surface of a third body, respectively. Understanding the mechanisms of nucleation in detail would give us greater scope to explore new phases of materials with unusual properties. A major factor that hinders us from studying nucleation is its stochastic nature; we generally can't predict where or when nucleation will take place. This hindrance is further exacerbated by the small length and time-scales involved.

The longest-standing theoretical model of nucleation is classical nucleation theory.[1, 2] This model considers the free-energy change for formation of a cluster, comprised of surface energy and bulk energy terms. The theory predicts a critical cluster size beyond which spontaneous growth can be sustained. The solution can be viewed as a dynamic system where clusters continually grow and dissolve, unit by unit, until chance creates a critical cluster. Classical nucleation theory does a remarkably good job; there are several criticisms of the theory, however. One major criticism is the use of bulk thermodynamic parameters, such as interfacial tension, to describe nanoscale clusters. Another problem is that the theory does not explicitly consider variations in cluster structure.[3]

A more promising approach to nucleation theory is the two-step mechanism.[2, 3] The first step involves formation of dense regions of solute or metastable clusters, which are considered to be liquid-like and may include solvent; the second step involves structural organisation or nucleation within these dense regions. A key feature of the mechanism is the incorporation of both concentration and structure co-ordinates in the free-energy pathway to nucleation. The mechanism is much more in accord with experiments on protein nucleation.[4-6] Current experimental and computational evidence suggest that the two-step nucleation mechanism is also applicable to small-molecule systems.[7]

Both the classical and two-step theories suggest a population of clusters of solute exist in solution prior to nucleation. There is a lot of circumstantial evidence to support the existence of these clusters for small-molecule systems, such as diffusivity measurements,[8] Raman spectroscopy,[9] small-angle neutron scattering,[10] static (Rayleigh) light scattering,[11, 12] and dynamic light scattering.[13-15] Other experiments, however, suggest that clustering is not at all prevalent.[10, 16]

Recently there has been much interest in the use of laser light to induce nucleation.[17-21] A comprehensive review of the methods and systems explored lies outside the scope of the present article, and the reader is directed elsewhere for more details.[20, 22] The method of non-photochemical laser-induced nucleation (NPLIN) is particularly interesting because it is believed to proceed without photomechanical or photochemical damage to the system.[17] NPLIN involves exposing supersaturated solutions or supercooled liquids to nanosecond-duration pulses of visible or near-infrared laser light.[23-25] The exact mechanism for NPLIN has not been resolved. The favoured theory is that the intense electric field ($\sim 10^7$ V m^{-1}) at the peak of the laser pulse interacts with the polarizability of clusters of solute molecules, causing them to re-structure to become critical nuclei.[17, 19, 26] NPLIN was discovered by accident: to quote Garetz et al.,[17]

"*Recently, while attempting to observe second harmonic generation in supersaturated solutions of urea in water, we have noticed that pulses from a Q-switched Nd:YAG laser can induce nucleation in such solutions*."

The observation of nucleation under those conditions was remarkable, but distracted attention from the original aim of the work.

Second-harmonic scattering (SHS) is a non-linear optical process that doubles the frequency of light.[27] In the electric-dipole approximation, bulk second-harmonic generation (SHG) requires the incoming and outgoing photons to be phase-matched in a material with a non-zero second-order susceptibility tensor $\chi^{(2)}$. This material is typically a single crystal from a class that is non-centrosymmetric, e.g., potassium titanyl phosphate (KTP, commonly used to convert near-infrared diode laser light to visible light in green laser pointers). Surface SHG is possible, even at the surfaces of centrosymmetric materials, due to the breaking of inversion symmetry at the interface. The disordered, homogeneous nature of an aqueous solution would be expected to preclude bulk SHG. However, SHS may also be observed in liquids due to hyper-Rayleigh scattering (HRS), which is caused by local density and orientation fluctuations.[28, 29]

There is only one known crystal polymorph of urea at ambient pressures.[30] The crystallographic space group is $P\bar{4}2_1m$, which is non-centrosymmetric and also second-harmonic active.[31, 32] If solute clusters do exist in solution: what is the structure of a typical cluster? Do the clusters have any ordered (e.g., crystalline) component, or are they disordered? In the case of urea, if these clusters have a crystalline component, it is very likely to be that of the known solid phase, and therefore second-harmonic active. SHS has recently been applied to monitor nucleation and growth of second-harmonic active materials.[33, 34] In order to test for the presence of clusters in aqueous (metastable) supersaturated urea solutions, we have re-visited the experiments of Garetz *et al*. to attempt to observe second-harmonic generation.

2. Experimental methods

The SHS microscope used was based on a fluorescence-lifetime imaging microscopy (FLIM) setup that has been described in detail previously.[35] The light source was a diode-pumped Ti:sapphire laser (Coherent, Verdi V18 and Mira F900) operating at 800 nm to produce 180 fs pulses at 75 MHz. The 800 nm pump beam was focussed through an inverted water-immersion microscope objective (×60, NA 1.2) onto the sample, which was mounted on a motor-controlled XY translational stage (Märzhäuzer Wetzlar GmbH & Co. KG, SCAN IM120×100). Photon emission was collected through the same objective and detected using an external fast micro-

channel plate photomultiplier tube (Hamamatsu, R3809U-50). Emission was recorded using time-correlated single photon counting (TCSPC) through a computer interface (Becker and Hickl, SPC830). Optical filters were employed to select the emission wavelength range detected. A visible band-pass filter (Schott glass, BG39) was used to block out the source light, while allowing detection of wavelengths in the range 340 – 610 nm. In addition, optional interference filters could be used to pass narrow bands at 400 ± 40, 450 ± 40, and 458 ± 10 nm (Comar Optics 400IU25, 450IU25 and 458IL25, respectively). The emission was detected without selection of polarization. Collection of emission in the forward direction was investigated using a second objective. It was found that the signals obtained were fractionally lower. The reduced signal may be attributed in some part to the difficulty in aligning un-matched objectives. Laser powers reported here were those measured before the objective: 1 mW corresponds to a single pulse peak power density of ~50 GW cm^{-2}.

Sample vessels were prepared by gluing glass rings (17mm diameter × 4mm tall) onto coverslips (No. 1.5) using optical glue (Norland, Optical Adhesive 61). Two samples of urea were used, one from VWR (BDH, AnalR grade) and the other from Sigma Aldrich (puriss p.a. ACS grade, 99.8%). The experiments were conducted at 21 °C: the saturation concentration of urea at this temperature was calculated to be C_{sat} = 18.14 mol kg^{-1}. Urea solution was hot-filtered through 0.22-μm syringe filters (Millex GS) and placed as a droplet onto the coverslip (volume ~0.02 cm^3) inside the glass ring; the sample vessel was sealed with another coverslip. A range of samples with supersaturations $S = C/C_{sat}$ from 0.15 to 1.86 at 21 °C were tested.

For comparative experiments, barium titanate nanoparticles ($BaTiO_3$, 99.9%, tetragonal phase) were purchased from Nanostructured and Amorphous Materials, Inc. (Houston, TX). The particles were approximately spherical, with mean diameter, d = 200 nm. The crystal space group of the tetragonal phase of $BaTiO_3$ is P4mm, which is non-centrosymmetric and second-harmonic active.[32, 36] To disperse the particles, 8 mg of $BaTiO_3$ powder was added to 11.6 g of urea solution (2.72 mol kg^{-1}) followed by shaking and sonication. 1.00 g of this crude stock dispersion was filtered through a 0.22-μm syringe filter into 8.50 g of urea solution (1.02 mol kg^{-1}). The resulting solution contained $BaTiO_3$ nanoparticles (d < 200 nm) in 1.19 mol urea kg^{-1}. Successful dispersion was verified using the microscope; no further analysis was carried out.

The data collection involved integrating the time-dependent TCSPC photon counts over a fixed period. In order to measure the photon signal over a large volume of the solution, the sample was placed on a motorised XY translational stage to allow scanning. A typical scan consisted of a series of translational steps: along the X direction for 1 mm followed by a 2 μm step in the Y

direction, and so on. Each 1 mm step in the X direction took ~2.25 s. The depth of the focal volume into the solution was typically 100 μm beyond the coverslip. The photon count was continually integrated during the scanning procedure.

3. Results

The microscope setup was optimized and tested using a sample of crushed, crystalline potassium dihydrogen phosphate (KDP) which gives a strong SHG response.[37] The TCSPC time-dependent photon count is shown in Fig. 1. The trace shows a very sharp response at time, t = 1 ns, which is the 400-nm second harmonic of the input pump light at 800 nm, and represents the instrument response function. The peak can be fitted using a single Gaussian function with full-width at half-maximum (FWHM) of 55 ps.

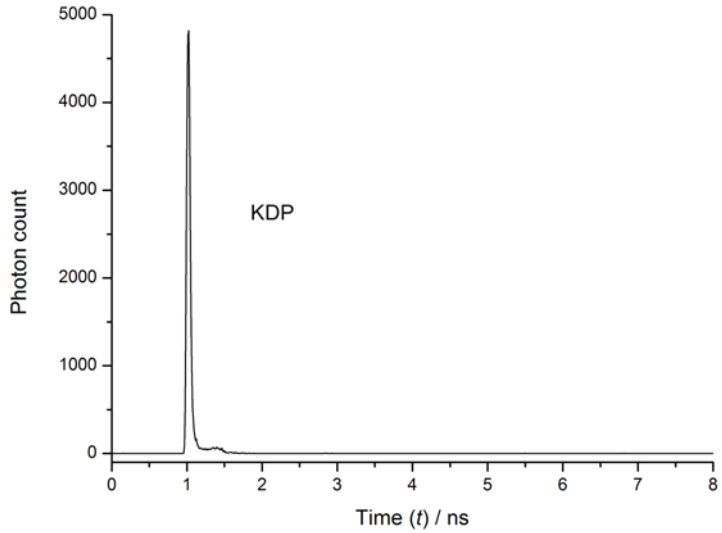

Fig. 1. Time-dependent photon count for solid potassium dihydrogen phosphate crystals. The peak is attributed to second-harmonic generation at 400 nm using an 800 nm pump-pulse train (laser power, P = 0.7 mW, 10 s integration). The shape of the peak represents the instrument response function, and can be fitted using a single Gaussian function with full-width at half-maximum (FWHM) of 55 ps.

Time-dependent photon counts obtained from water and from slightly undersaturated urea solution (S = 0.98) are shown in Fig. 2. The water trace (2c) was obtained using the visible band-pass filter and shows no clear peak at t = 1 ns. The urea trace obtained using a narrow-pass filter at 400 nm (2a) shows a sharp peak. The peak was fitted using a single Gaussian function with FWHM of 43 ps, which is close to the value obtained for KDP (Fig. 1). The urea trace taken using a narrow-pass filter at 458 nm (2b) shows no peak, supporting the assignment of the emission as SHS from

the urea solution. The results in Fig. 2 demonstrate that, under similar conditions, a second-harmonic signal was obtained from urea solution but not from water.

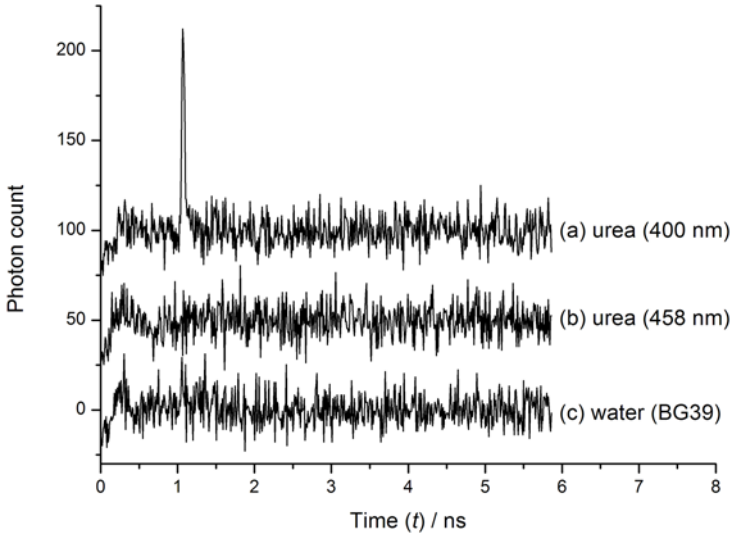

Fig. 2. Time-dependent photon counts for undersaturated urea solutions (S = 0.98) and water. All traces were integrated for 180 s while scanning the beam through the droplet using identical pump laser powers (P = 3.8 mW). The background level of each trace has been offset to aid comparison. Trace (c), for water, was acquired using a visible band-pass filter (BG39). The top two traces were acquired for urea solution using (a) 400 ± 40 nm and (b) 458 ± 10 nm interference filters, respectively. The peak in (a) can be fitted using a Gaussian function with FWHM of 43 ps.

We conducted several tests to verify that the signal observed was consistent with SHS from the solution, and not from other sources. We verified that the total SHS signals ($I_{2\omega}$) from both water and from urea solution (S = 0.98) showed a quadratic dependence on incident intensity (I_0), $I_{2\omega}^{(\mathrm{SHS})} \propto I_0^2$. One potential artefact could be multiphoton-induced breakdown of the liquid, resulting in plasma emission at the focal volume. We would expect the plasma emission to have a similar temporal profile to SHS. We note, however, that the power densities employed here are orders of magnitude lower than would be required to cause breakdown.[38] Plasma emission was ruled out by using the interference filters to show that the emission contained a very narrow range of wavelengths at 400 nm rather than a broad band in the UV–blue region of the spectrum.

Other potential artefacts include extrinsic sources of SHG, e.g., from the coverslip, or at the coverslip–droplet or droplet–vapour interfaces. At the laser powers (P = 3.8 mW) used to obtain the traces in Fig. 2, a small signal was observed using only water when the excitation beam was focussed directly onto the coverslip–droplet interface. Moving the focal volume into the liquid by ~20 μm was sufficient to remove this signal. Raising the laser power to P = 10 mW a small signal

was obtained even at ~20 μm into the droplet. The signal was found to decrease with increasing depth into the droplet, and therefore we attribute it to surface SHG from the droplet–coverslip interface. All of the measurements on urea reported here were carried out at sufficient powers (P < 4.0 mW) and depths (~100 μm) to avoid interference from this interfacial SHG; conditions were verified periodically throughout the experiments.

We attempted to detect SHS from both glycine and sucrose solutions. In each case a long decay signal was observed, masking any SHS, as shown in Fig. 3. The cause of this 2-photon fluorescence is not clear, since there are no electronic states of glycine at the right energy.[39] It may be possible that fluorescence arises due to glycine aggregation at these high concentrations. We did not pursue further analysis of these systems for the present work, and in the absence of further data we attribute the emission to trace impurities in the sample used.

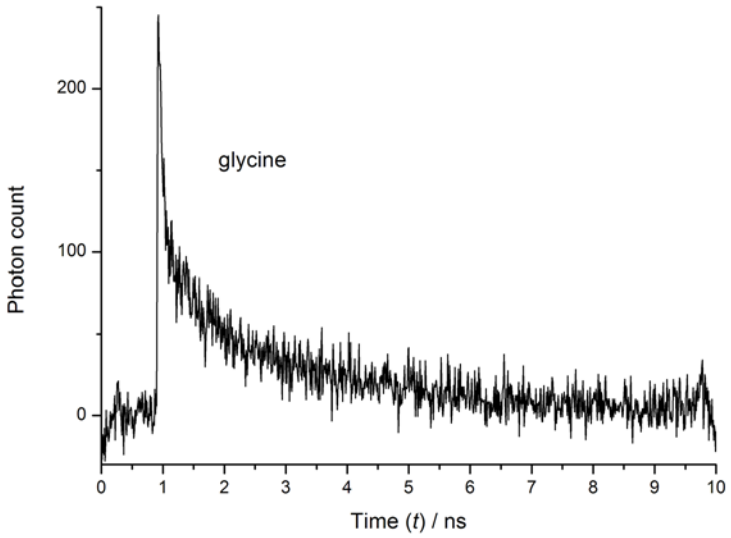

Fig. 3. Time-dependent photon count for undersaturated glycine solution (S = 0.95). The pump-laser power was P = 4.0 mW and signal was integrated for 180 s while scanning through solution. The decay of the trace can be fitted with two exponential functions (lifetimes, τ_1 = 0.16 ns and τ_2 = 2.16 ns).

In Fig. 4 we show results for detection of SHS from urea solutions with supersaturations ranging from S = 0.15 (undersaturated) to S = 1.86 (highly supersaturated). The signal is seen to increase with concentration up to the point of saturation (S = 0.95) and then decrease up to S = 1.35; the signal then increases again up to S = 1.75, and drops again at the highest supersaturation (S = 1.86). Repeat measurements were made with samples tested in a random order. There were no signs of nucleation or damage to samples. The dependence of the signal on concentration does not increase monotonically, as would be expected for hyper-Rayleigh scattering,[40] and is strong evidence that the signal that we have measured is intrinsic, i.e., it originates from the structure of

the urea solution. The most remarkable feature is the apparent turnover near saturation (S = 1): this is the cross-over point where the solution becomes metastable, where we might expect the structure of the solution to change. The results accord well with Guoy interferometry measurements of Sorell and Myerson, who saw a sharp decrease in urea diffusivity above saturation, which they attributed to the formation of larger urea clusters.[8]

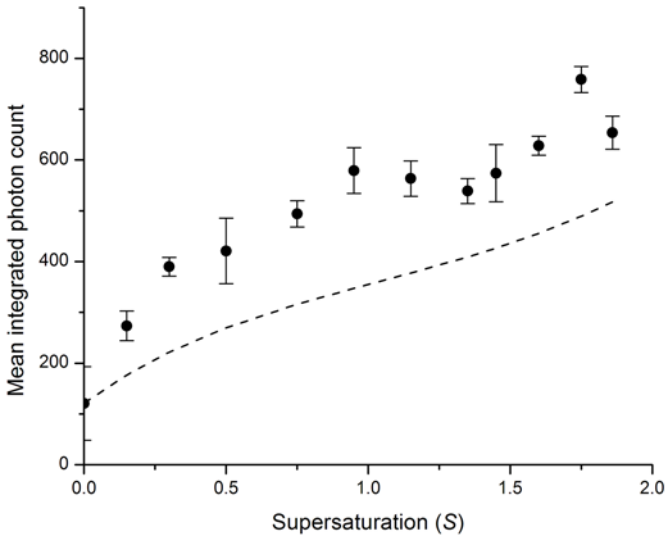

Fig. 4. Concentration dependence of SHS signal from urea solutions. The pump-laser power was P = 3.8 mW, and the depth was ~100 μm. Emission was detected while scanning the focal volume through the solution, integrating for 180 s per trace. For each trace, a baseline signal was calculated by averaging data from 2 to 3 ns (*cf.* Fig. 2) and this was subtracted from the data. The total photon count under the peak was integrated. The mean value of these signal counts, calculated from repeat measurements, is plotted on the vertical axis. Error bars represent 95% confidence intervals from the repeat measurements. The dashed line represents model calculations of hyper-Rayleigh scattering, which have been scaled by a constant factor to match the experimental data at the point S = 0 (water).

The influence of hyper-Rayleigh scattering was determined as follows. Scattered HRS intensity can be written as $I_{2\omega}^{(\mathrm{HRS})} = G I_0^2 B^2$, where ($I_0$) is the incident intensity and G is a constant containing geometrical and electric-field factors.[40] The HRS scattering term B^2 can be expanded as

$$B^2 = N_{\mathrm{urea}} \left\langle \beta_{\mathrm{urea}}^2 \right\rangle + N_{\mathrm{water}} \left\langle \beta_{\mathrm{water}}^2 \right\rangle \qquad (1)$$

where N_{urea} and N_{water} are the molecule number densities of urea and water, respectively. The space-averaged first-order hyperpolarizabilities for each molecule are given by $\left\langle \beta^2 \right\rangle = \left\langle \beta_{ZZZ}^2 \right\rangle + \left\langle \beta_{XXZ}^2 \right\rangle$, which represent laboratory-frame averages over the molecule-frame hyperpolarizabilities.[41] Using theoretical values of molecule-frame hyperpolarizabilities (β_{xxz}, β_{yyz}, β_{zzz}) for water[42] and for urea[43] (both have C_{2v} symmetry) we calculated $\left\langle \beta_{\mathrm{urea}}^2 \right\rangle = 0.14 \times 10^{-30}$ esu and $\left\langle \beta_{\mathrm{water}}^2 \right\rangle = 0.011 \times 10^{-30}$ esu.

We used these values to calculate the concentration dependence of B^2, taking into account the change in solution density with concentration.[44] The results are shown as the dashed curve in Fig. 4; the curve has been scaled by a constant factor to match the experimental results at $S = 0$ (water). Ignoring the arbitrary scaling factor, the overall trend in the HRS scattering model matches the increasing signal with concentration observed in the experimental data. However, at higher concentrations, the experimental SHS deviates significantly from the model.

Rayleigh scattering measurements, similar to those of Li and Ogawa on KDP and KCl solutions,[12] reveal a population of particles in urea solutions: see Fig. 5.[45] To determine if the features in the experimental data shown in Fig. 4 could be attributed to SHG from floating particles, we lowered the data-acquisition integration time to 0.2 s, to acquire a sequence of traces while scanning through the solution. This integration time corresponds to an X displacement of 90 μm. In Fig. 6(a) we show the results from a sequence of 2000 traces for urea ($S = 0.98$). Each point in this figure represents the integrated photon count from the emission peak. In Fig. 6(b) we show the total time-dependent photon-count obtained by summing up all traces. The total trace shows a clear peak. Fig. 6(a) demonstrates that the SHS signal we have observed is caused by individual events encountered while scanning through the solution. This further strengthens the case for the signal as being intrinsic to the solution, and not an artefact from the coverslip or elsewhere in the system.

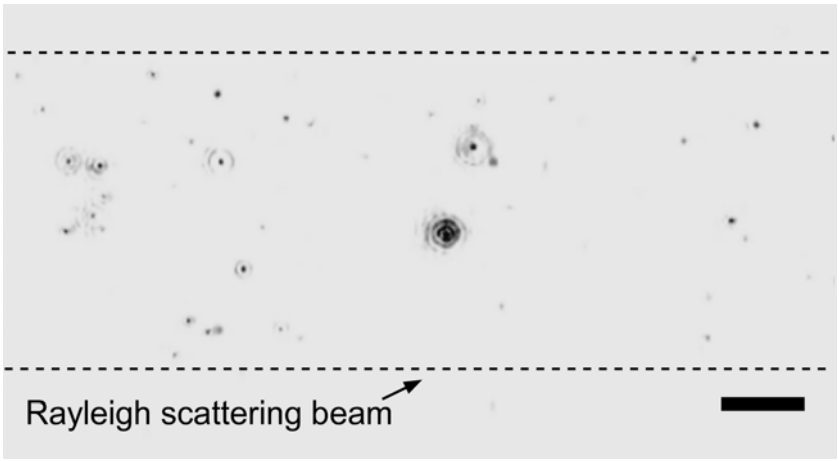

Fig. 5. Rayleigh scattering image of undersaturated urea solution ($S = 0.95$). The 488 nm beam ($P = 55$ mW) was focussed into solution using a lens (focal length = +200 mm) and the Rayleigh scattering imaged at right angles through an objective (×50). Because the dimensions of the particles are much smaller than the wavelength of scattered light, the particles can be considered as point sources and appear in the image as concentric rings (point spread function). The scale bar (bottom right) represents 10 μm.

The scan for the results in Fig. 6 took approximately 400 s to complete, and the effective distance travelled was ~0.18 m. If we assume a focal-volume width of 400 nm and depth of 600 nm,

the total volume probed during the scan was 4.3×10^{-14} m^3. Setting an arbitrary threshold, we count 7 peaks in Fig. 5(a). This equates to roughly 1.6×10^8 particles cm^{-3}. This estimate is comparable to that obtained by Lian et al., who measured 1.3×10^6 particles cm^{-3} for supersaturated KDP solution (S = 1.001) using Rayleigh scattering.[46] Jawor–Baczynska et al. report estimates of 10^9 particles cm^{-3} in their studies of supersaturated (S = 1.08) glycine solutions.[15] Our Rayleigh scattering measurements suggest densities of 2.9×10^8 particles cm^{-3},[45] close to the value estimated here.

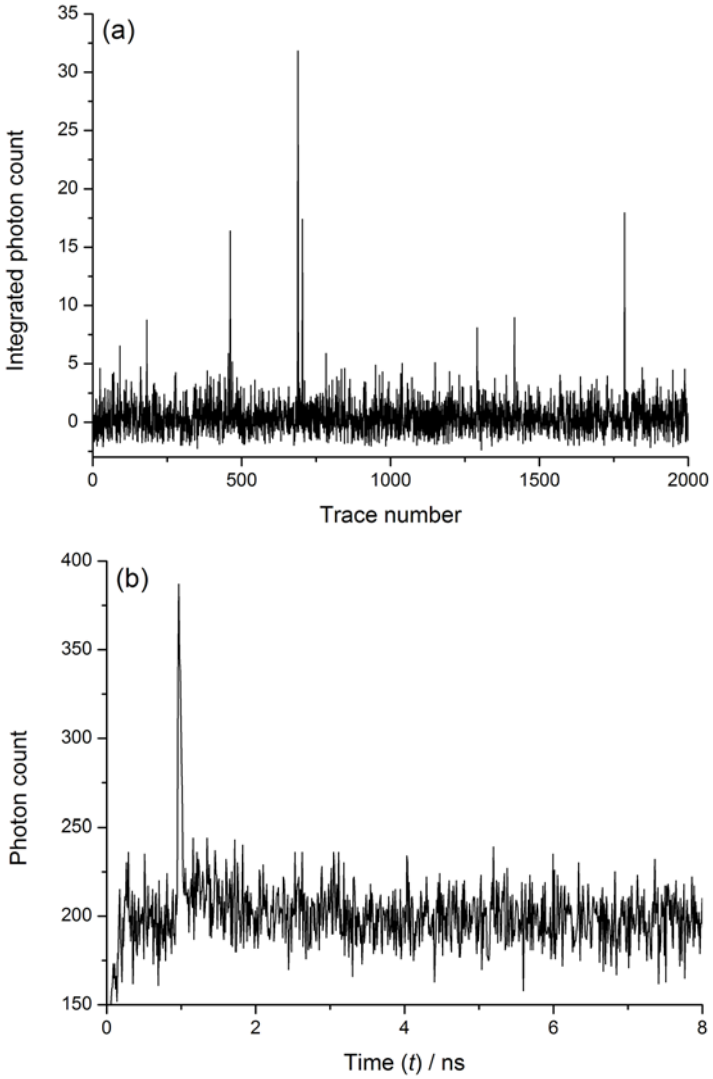

Fig. 6. (a) Integrated peak photon counts from a series of traces taken while scanning through urea solutions (S = 0.98). The integration time for each trace was 0.2 s. The signal under the peak for each trace was integrated as detailed in Fig. 4. The pump-laser power was P = 3.4 mW. The total signal from summing over all 2000 traces is shown in (b). The peak at ~1 ns is the SHS signal. The results suggest that the total signal originates from individual peak events detected while scanning through the solution.

To make comparisons with particulate material that is known to be SHG-active, we carried out scanning measurements on dispersions of $BaTiO_3$ nanoparticles.[47] In Fig. 7(a) we show a direct comparison between integrated peak photon counts for $BaTiO_3$ and for urea solution ($S = 0.98$). The integration time for each trace was 10 s. Two consecutive traces taken for the urea sample are shown in Fig. 7(b) to illustrate the contribution that a single event makes to the overall signal. Similar scans for water samples did not show spikes like those seen for $BaTiO_3$ and urea samples. The peaks from the $BaTiO_3$ scan are approximately 20 times larger than those from urea.

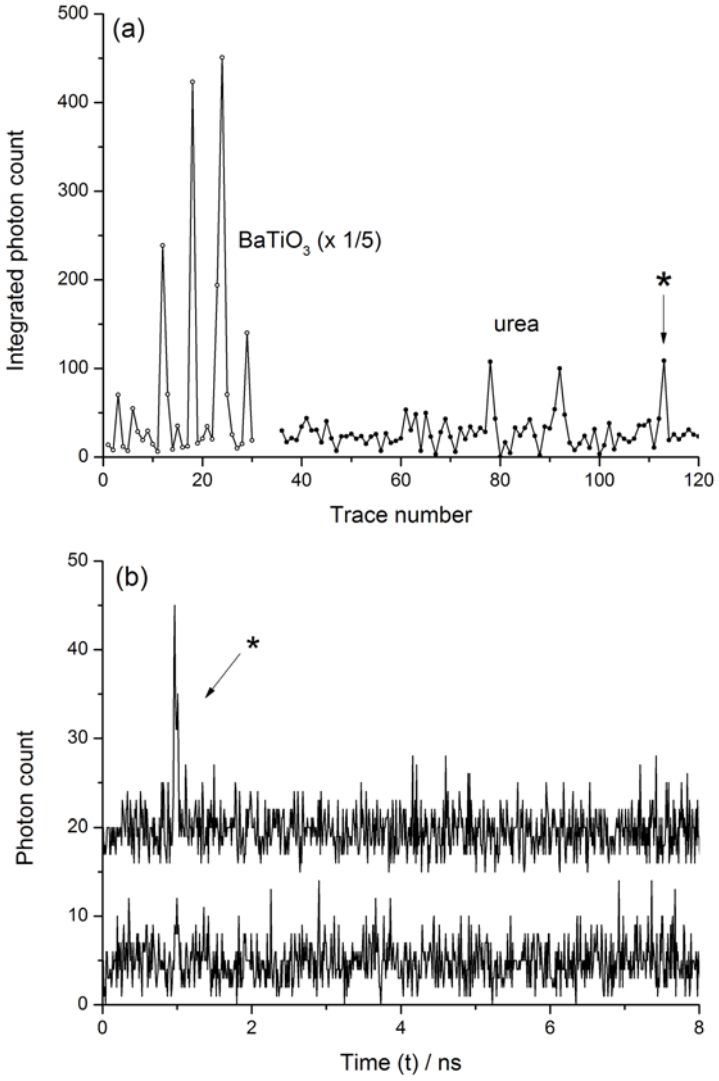

Fig. 7. (a) Integrated photon counts from a series of traces taken while scanning through the solutions; these are total counts obtained by integrating under the peak for each trace, as described in Fig. 4. The integration time for each trace was 10 s. The first set of 30 points (open circles) were obtained using a dispersion of $BaTiO_3$ nanoparticles with diameters $d < 200$ nm; laser power $P = 3.8$ mW. The $BaTiO_3$ data have been multiplied by a factor of 1/5 to plot them on the same scale. The second set of points (closed circles) from 36 – 120 were taken using urea solution ($S = 0.98$); laser power $P = 3.4$ mW. In (b)

we show individual traces, numbers 113 (marked with an asterisk *) and 114; the top trace has been offset (by 15 counts) to aid comparison.

4. Discussion

The results shown in Figs 4–7 suggest that the SHS signal we observe is dominated by clusters floating in solution. At supersaturation (S = 1.0), the mole fraction of urea is x = 0.33, i.e., nearly one-third of molecules is solute; at S = 1.86, we have x = 0.61. Clusters are liable to form due to the competition between solute–solute interactions and solute–solvent (and also solvent–solvent). As the concentration increases, the persistence (lifetime) and size of these clusters would be expected to increase.

The bulk SHG efficiency (η) of urea relative to quartz (η = 400) is similar to that of $BaTiO_3$ (η = 130).[37] Taking the efficiency factor into account, the signal from $BaTiO_3$ nanoparticles (d < 200 nm), is a factor of 60 larger than signals for nearly saturated urea solution. If clusters of urea do have a crystalline structure, this factor could simply be due to the smaller size of the urea particles. For bulk SHG, considering the dependence of SHG conversion efficiency on the interaction length (L), and taking into account the cross-sectional area of the particles illuminated (σ), we calculate $\eta_{2\omega}^{(SHG)} \propto L^2\sigma$.[48] For a particle of diameter d, $\eta_{2\omega}^{(SHG)} \sim d^4$, and we estimate that the particles of urea would be 2.8 times smaller than the equivalent $BaTiO_3$ particles. This is a very crude estimate, however.

The mechanism for second harmonic generation from nanoparticles is distinct from bulk SHG. Since the particle is very much smaller than the wavelength of the exciting radiation, the mechanism is analogous to HRS. The incident electric field induces local dipoles (and multipoles) in and around the nanoparticle. The contributions from the induced dipoles combine coherently to produce the resulting SHG.[49] SHG can therefore be considered as a signature of locked-in order, e.g., in particles, as compared to statistical fluctuations that result in HRS.

Bulk and surface SHG generate similar lifetimes and we are unable to assign whether SHG originates from native urea clusters or an unknown impurity. We consider each of the possible sources in turn.

(1) Bulk: For nanoparticles of non-centrosymmetric materials, bulk SHG has been demonstrated to be very efficient.[47, 50] The peak signals that we measured for urea are only 1–2 orders of magnitude lower than for SHG-active $BaTiO_3$ nanoparticles. As outlined above, this

reduction may be due to crystalline clusters of urea that are smaller than the $BaTiO_3$ nanoparticles. We note that full crystalline order is not required for bulk SHG: all that is required is some non-centrosymmetric orientational order from the urea molecules at these length scales.[49] Electronic structure calculations on small urea clusters (up to the septimer) show near-linear additivity in the hyperpolarizability, and also highlight the importance of contributions from hydrogen bonding.[51] The changes in SHS with concentration, shown in Fig. 4, could originate from changes in the internal structures or number densities of semi-ordered clusters.

(2) Surface: If the core of a urea cluster is completely centrosymmetric (e.g., disordered), the bulk contribution to SHG vanishes. SHG can then take place due to the breaking of inversion symmetry at the cluster–solution interface. For a spherical cluster, the integrated surface contribution vanishes. In the present case, surface SHG could occur in two ways: (i) from non-spherical clusters or (ii) from clusters that are spherical but with an outer shell of molecules having some degree of orientational order.[52]

(3) Impurities: SHG due to solid impurity particles essentially follows the mechanisms (1) and (2) above. It is possible that the impurity happens to be SHG active. Alternatively, even for spherical centrosymmteric impurities, the orientational order of urea molecules adsorbed onto the particle could produce surface SHG.[52] At the high urea concentrations employed, we would expect the surface coverage of the particles to be saturated, even at $S = 0.15$. Assuming that any impurities come from the urea, the SHG for either case (bulk or surface) would be expected to increase linearly with concentration, contrary to our observations (Fig. 4). It is always possible, however, that the impurity particles induce some order in the surrounding solution. We note that no impurities were detected in water samples prepared in an identical way.

The sources of SHG listed above share a common feature, *viz*. that increasing orientational order of the solute molecules increases the second harmonic scattering. At the present time it is not clear why the SHS signal (Fig. 4) appears to dip in the region above $S = 1.0$ and again at $S = 1.7$. One explanation is that we are measuring changes in the orientational order *and* number density of clusters, both of which change with concentration. At the point of supersaturation ($S = 1.0$), we might expect larger clusters to favoured. Our signal would be higher when there are many small clusters that are more frequently encountered during the scanning of the focal volume through the solution; as concentration is increased these may transform to larger clusters, which we are less likely to encounter. We might consider the changes at $S = 1.0$ and 1.7 as spinodal decomposition, effectively separation of a distinct phase that is metastable and disordered, and which relieves the increasing burden on the water molecules to satisfy their role as solvent.

Further work is required to support the preliminary results presented here. This could include correlating SHS with Rayleigh scattering measurements to demonstrate that the peak signals come from long-lived particles. Perhaps more-challenging will be to measure angle-dependent scattering, to separate coherent SHG scattering from incoherent HRS, and thereby to determine more details of the structure of the scattering particles.

5. Conclusions

In summary, we have demonstrated measurements of second-harmonic scattering (SHS) from aqueous solutions of urea using scanning microscopy. SHS was measured as a function of solute concentration ranging from $S = 0.15$ (undersaturated) to $S = 1.86$ (supersaturated). The results show an overall increase in the SHS signal with concentration; local maxima near $S = 0.95$ and 1.75 suggest significant changes in the solution structure at these concentrations. Rayleigh scattering experiments indicate a population of free particles in aqueous urea solutions. Time-dependent SHS experiments revealed distinct peaks in SHS signal while scanning the focal volume through solution. These peaks are consistent with SHG from particles; similar peaks were observed when scanning through aqueous dispersions of $BaTiO_3$ nanoparticles that are known to exhibit bulk second harmonic generation (SHG). SHG intensities from the $BaTiO_3$ nanoparticles (diameters, $d <$ 200 nm) were ~20 times greater than from urea solution ($S = 0.98$). Our experiments suggest that semi-ordered urea clusters exist in aqueous urea solutions, and that the structures and number densities of these clusters change with concentration.

Acknowledgements

AJA is grateful to Dr Philip Camp (Edinburgh) for useful discussions. We wish to acknowledge the Science and Technology Facilities Council (STFC) and the Engineering and Physical Sciences Research Council (EPSRC) for supporting this work (EP/G067546/1), and to the Royal Society (London) for a research grant.

References

1. J. W. Mullin, *Crystallization*, Butterworth-Heinemann, Oxford, 2001.
2. D. Erdemir, A. Y. Lee and A. S. Myerson, *Accounts Chem. Res.*, 2009, **42**, 621-629.
3. P. G. Vekilov, *Cryst. Growth Des.*, 2010, **10**, 5007-5019.
4. D. Vivares, E. W. Kaler and A. M. Lenhoff, *Acta Cryst. D*, 2005, **61**, 819-825.
5. P. R. ten Wolde and D. Frenkel, *Science*, 1997, **277**, 1975-1978.

6. O. Galkin, K. Chen, R. L. Nagel, R. E. Hirsch and P. G. Vekilov, *PNAS*, 2002, **99**, 8479-8483.
7. D. Zahn, *Phys. Rev. Lett.*, 2004, **92**, 040801.
8. L. S. Sorell and A. S. Myerson, *AIChE J.*, 1982, **28**, 772-779.
9. R. L. Frost and D. W. James, *J. Chem. Soc. Faraday Trans.*, 1982, **78**, 3223-3234.
10. P. E. Mason, G. W. Neilson, S. R. Kline, C. E. Dempsey and J. W. Brady, *J. Phys. Chem. B*, 2006, **110**, 13477-13483.
11. L. Lian, T. J. Lu, Y. Zaizu and T. Ogawa, *J. Mater. Res.*, 1996, **11**, 387-390.
12. L. Li and T. Ogawa, *J. Cryst. Growth*, 2000, **211**, 286-289.
13. Y. Georgalis, A. M. Kierzek and W. Saenger, *J. Phys. Chem. B*, 2000, **104**, 3405-3406.
14. M. Sedlák, *J. Phys. Chem. B*, 2006, **110**, 4329-4338.
15. A. Jawor-Baczynska, J. Sefcik and B. D. Moore, *Cryst. Growth Des.*, 2012, **13**, 470-478.
16. J. Huang, T. C. Stringfellow and L. Yu, *J. Am. Chem. Soc.*, 2008, **130**, 13973-13980.
17. B. A. Garetz, J. E. Aber, N. L. Goddard, R. G. Young and A. S. Myerson, *Phys. Rev. Lett.*, 1996, **77**, 3475-3476.
18. B. A. Garetz, J. Matic and A. S. Myerson, *Phys. Rev. Lett.*, 2002, **89**, 175501.
19. A. J. Alexander and P. J. Camp, *Cryst. Growth Des.*, 2009, **9**, 958-963.
20. T. Sugiyama, K.-I. Yuyama and H. Masuhara, *Accounts Chem. Res.*, 2012, **45**, 1946-1954.
21. S. Nakayama, H. Y. Yoshikawa, R. Murai, M. Kurata, M. Maruyama, S. Sugiyama, Y. Aoki, Y. Takahashi, M. Yoshimura, S. Nakabayashi, H. Adachi, H. Matsumura, T. Inoue, K. Takano, S. Murakami and Y. Mori, *Cryst. Growth Des.*, 2013, **13**, 1491-1496.
22. M. R. Ward and A. J. Alexander, *Cryst. Growth Des.*, 2012, **12**, 4554-4561.
23. M. R. Ward, G. W. Copeland and A. J. Alexander, *J. Chem. Phys.*, 2011, **135**, 114508.
24. M. R. Ward, S. McHugh and A. J. Alexander, *Phys. Chem. Chem. Phys.*, 2012, **14**, 90-93.
25. C. Duffus, P. J. Camp and A. J. Alexander, *J. Am. Chem. Soc.*, 2009, **131**, 11676-11677.
26. M. R. Ward, I. Ballingall, M. L. Costen, K. G. McKendrick and A. J. Alexander, *Chem. Phys. Lett.*, 2009, **481**, 25-28.
27. R. W. Boyd, *Nonlinear optics*, Academic Press, London, 2003.
28. R. W. Terhune, P. D. Maker and C. M. Savage, *Phys. Rev. Lett.*, 1965, **14**, 681-684.
29. P. D. Maker, *Phys. Rev. A*, 1970, **1**, 923-951.
30. P. W. Bridgman, *Proc. Am. Acad. Arts Sci.*, 1916, **52**, 91-187.
31. S. Swaminathan, B. M. Craven and R. K. McMullan, *Acta Cryst. B*, 1984, **40**, 300-306.
32. T. Hahn, ed., *International tables for crystallography, Volume A*, D. Reidel, Dordrecht, 1983.

33. M. C. D'Arrigo, F. R. Cruickshank, D. Pugh, J. N. Sherwood, J. D. Wallis, C. Mackenzie and D. Hayward, *Phys. Chem. Chem. Phys.*, 2006, **8**, 3761-3766.
34. D. Segets, L. Martinez Tomalino, J. Gradl and W. Peukert, *J. Phys. Chem. C*, 2009, **113**, 11995-12001.
35. S. W. Botchway, A. W. Parker, R. H. Bisby and A. G. Crisostomo, *Microscopy Res. Tech.*, 2008, **71**, 267-273.
36. J. P. Dougherty and S. K. Kurtz, *J. Appl. Cryst.*, 1976, **9**, 145-158.
37. S. K. Kurtz and T. T. Perry, *J. Appl. Phys.*, 1968, **39**, 3798-3813.
38. A. Vogel, J. Noack, G. Hüttman and G. Paltauf, *Appl. Phys. B*, 2005, **81**, 1015-1047.
39. R. Maul, M. Preuss, F. Ortmann, K. Hannewald and F. Bechstedt, *J. Phys. Chem. A*, 2007, **111**, 4370-4377.
40. K. Clays and A. Persoons, *Phys. Rev. Lett.*, 1991, **66**, 2980-2983.
41. S. J. Cyvin, J. E. Rauch and J. C. Decius, *J. Chem. Phys.*, 1965, **43**, 4083-4095.
42. A. V. Gubskaya and P. G. Kusalik, *Mol. Phys.*, 2001, **99**, 1107-1120.
43. T. Pluta and A. J. Sadlej, *J. Chem. Phys.*, 2001, **114**, 136-146.
44. D. Lide, ed., *CRC Handbook of Chemistry and Physics, 86th Edition*, CRC Press, Boca Raton, FL, 2005.
45. M. R. Ward, A. D. Ward and A. J. Alexander, unpublished work.
46. L. Lian, L. Taijing, K. Sakai and T. Ogawa, *J. Mater. Res.*, 1992, **7**, 3275-3279.
47. C.-L. Hsieh, Y. Pu, R. Grange and D. Psaltis, *Opt. Express*, 2010, **18**, 11917-11932.
48. B. E. A. Saleh and M. C. Teich, *Fundamentals of photonics*, John Wiley & Sons, Inc., Hoboken, NJ, 1991.
49. S. Wunderlich, B. Schürer, C. Sauerbeck, W. Peukert and U. Peschel, *Phys. Rev. B*, 2011, **84**, 235403.
50. L. Le Xuan, C. Zhou, A. Slablab, D. Chauvat, C. Tard, S. Perruchas, T. Gacoin, P. Villeval and J.-F. Roch, *Small*, 2008, **4**, 1332-1336.
51. K. Wu, J. G. Snijders and C. Lin, *J. Phys. Chem. B*, 2002, **106**, 8954-8958.
52. S.-H. Jen, G. Gonella and H.-L. Dai, *J. Phys. Chem. A*, 2009, **113**, 4758-4762.